Available online at www.sciencedirect.com
SCIENCE DIRECT®
Nuclear Instruments and Methods in Physics Research A 499 (2003) 167–190
NUCLEAR INSTRUMENTS & METHODS IN PHYSICS RESEARCH Section A
www.elsevier.com/locate/nima

The KEKB injector linac

I. Abe, N. Akasaka[1], M. Akemoto, S. Anami, A. Enomoto*, J. Flanagan, S. Fukuda, H. Fukuma, Y. Funakoshi, K. Furukawa, H. Hanaki[1], H. Honma, N. Iida, M. Ikeda, K. Kakihara, N. Kamikubota, T. Kamitani, H. Katagiri, T. Kawamoto, M. Kikuchi, H. Kobayashi, H. Koiso, T. Matsumoto, S. Michizono, K. Nakahara[1], H. Nakajima, K. Nakao, Y. Ogawa, Y. Ohnishi, S. Ohsawa, K. Oide, T. Oogoe, Y. Otake[1], I. Sato[1], K. Satoh, T. Shidara, A. Shirakawa, M. Suetake, T. Suwada, T. Urano[1], S. Yamaguchi, Y. Yano

High Energy Accelerator Research Organization (KEK), 1-1 Oho, Tsukuba, Ibaraki 305-0801, Japan

Abstract

An 8-GeV electron/3.5-GeV positron injector for KEKB was completed in 1998 by upgrading the existing 2.5-GeV electron/positron linac. The main goals were to upgrade its accelerating energy from 2.5 to 8 GeV and to increase the positron intensity by about 20 times. This article describes not only the composition and features of the upgraded linac, but also how these goals were achieved, by focusing on an optics design and commissioning issues concerning especially high-intensity single-bunch acceleration to produce positron beams.

PACS: 29.20

Keywords: Electron; Positron; Injector; Linac

1. Introduction

An electron/positron injector linac at KEK, capable of providing electrons at an energy up to 8 GeV and positrons up to 3.5 GeV, is used as a multi-purpose injector not only for the KEK B Factory (KEKB), but also for the Photon Factory (PF). At present, it delivers full-energy beams of 8-GeV electrons to the KEKB High-Energy Ring (HER) and 3.5-GeV positrons to the Low-Energy Ring (LER) using the entire linac. Further, beams of 2.5-GeV electrons are provided for the PF two light sources (the PF and the PF–AR) using a gun installed halfway of the linac.

The linac was originally constructed as a 2.5-GeV injector for the PF in 1982 [1–3]; a positron source was later added for the TRISTAN electron/positron collider [4]. However, this old linac was extensively reconstructed for the B-Factory project during 1994–1998 [5]. The two essential goal of this upgrade were to achieve an electron beam energy of 8 GeV and a single-bunch positron intensity of 0.6 nC. The former goal has been

*Corresponding author.
E-mail address: atsushi.enomoto@kek.jp (A. Enomoto).
[1] Presently left from KEK.

0168-9002/03/$ - see front matter
PII: S0168-9002(02)01787-4

accomplished by increasing both the linac length (from 400 to 600 m) and the acceleration field strength (from 8 to 20 MV/m), and the latter by increasing the primary electron energy (from 250 to 3.7 GeV) with high-intensity electron beams (10 nC/bunch).

The linac is shaped like a "J" as shown in Fig. 1, because the land was not enough to extend the linac straight. Two linacs are linked by a 180° bending beam transport (called J-arc). The whole linac consists of 55 S-band (2856 MHz) main accelerator modules, with a pre-injector (#A-1), a positron capture module (#2-1), and a module for energy-compression system (ECS) for positron beams. Seventeen upstream modules were newly constructed for KEKB. Each of the main accelerator module provides an average energy gain of 160 MeV.

The linac presently serves four rings by switching the beam modes. In the positron-beam mode, a radiator is inserted into the beamline at the half point of the linac. A large number of parameters, such as in the magnets and rf phases, are automatically switched from one mode to the other.

Since December, 1998, when KEKB commissioning started, injection from the linac has been successfully performed [6]. By sharing the injection time for KEKB and the PF/AR without interference and saving injection time, the linac has greatly contributed to the integrated luminosity in B-physics experiments. Table 1 gives the main design beam parameters and the results achieved so far.

2. Beam optics and dynamics

Several issues concerning beam optics and dynamics in realizing a high-intensity, single-bunched, primary electron beam for positron production as well as in the beam transport of a secondary positron beam and an 8-GeV, low-intensity electron beam are discussed in this section. Special emphasis is laid on the space-charge and wake-field effects caused by a high-intensity beam in a bunching section and regular acceleration sections [7].

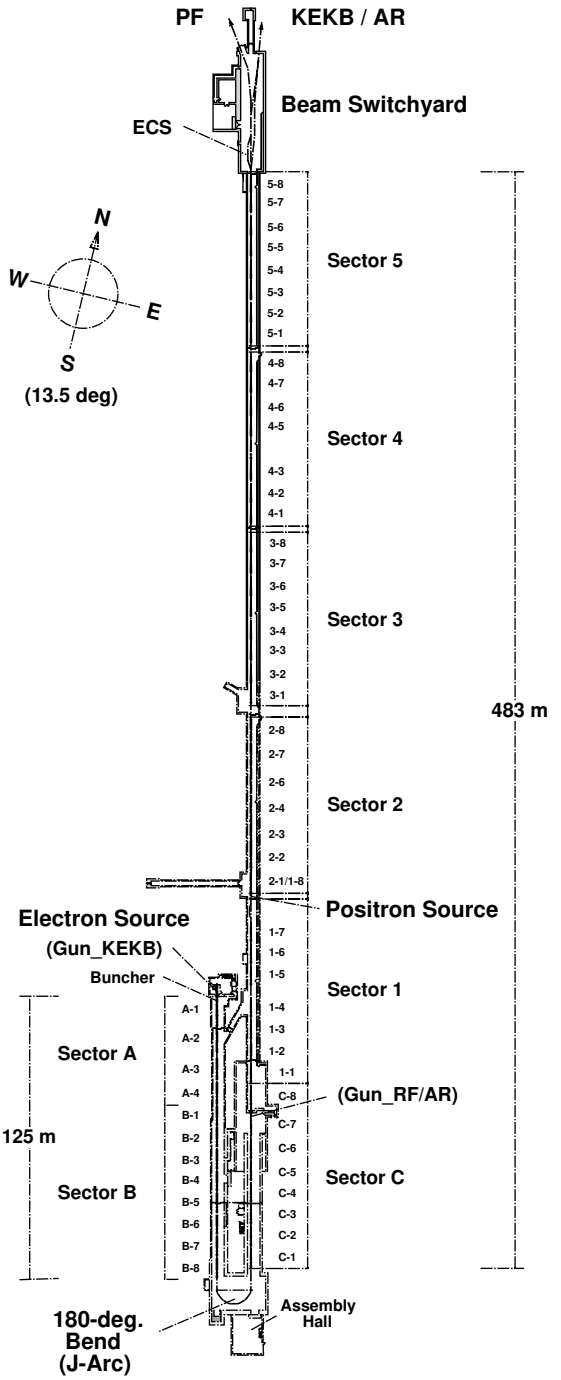

Fig. 1. Overall layout of the KEK electron/positron linac.

Table 1
Linac design beam parameters and performance

			8-GeV electron		3.5-GeV positron	
			Goal	Achieved	Goal	Achieved
(1) Gun	Energy	keV	200	200	200	200
	Intensity	nC/pulse	1.5	2	13	14
	Pulse width	ns	2	1.8	2	2.8
(2) Buncher	Energy	MeV	16	16	15	15
	Energy spread (σ)	MeV			2	2
	Intensity	nC/pulse	1.4	1.9	> 10	11
	Efficiency			95%		80%
	Emittance $\gamma\beta\varepsilon$ (σ)	mm	0.06	0.04	0.06	0.08
	Bunch width (σ)	ps	2.1	2.5	6.7	4.2
(3) Arc	Energy	GeV	1.5	1.7	1.5	1.7
	Energy spread (σ)	MeV	0.6%	0.29%	0.6%	0.38%
	Jitters (p–p)					0.1%
	Drift (with feedback)					<0.2%/h
	Emittance $\gamma\beta\varepsilon$ (σ)	mm		0.17		1.7
	Transmission			100%	> 95%	100%
(4) e + target	Energy	GeV			3.7	3.7
	Intensity	nC/pulse			> 10	10
	Transmission					90%
(5) e + Solenoid exit	Intensity	nC/pulse				2.4
	Specific yield	e^+/e^- GeV				6.5%
(6) Linac end	Energy	GeV	8	> 8	3.5	> 3.5
	Energy spread (σ)	MeV	0.15%	0.05%	0.125%	0.15%
	Intensity	nC/pulse	1.28	> 1.28	> 0.64	0.82
	Specific yield	e^+/e^- GeV				2.3%
	Transmission			> 70%		
	Emittance $\gamma\beta\varepsilon$ (σ)	mm	0.25	0.31	1.5	1.4
	Pulse repetition	pps	50	50	50	50

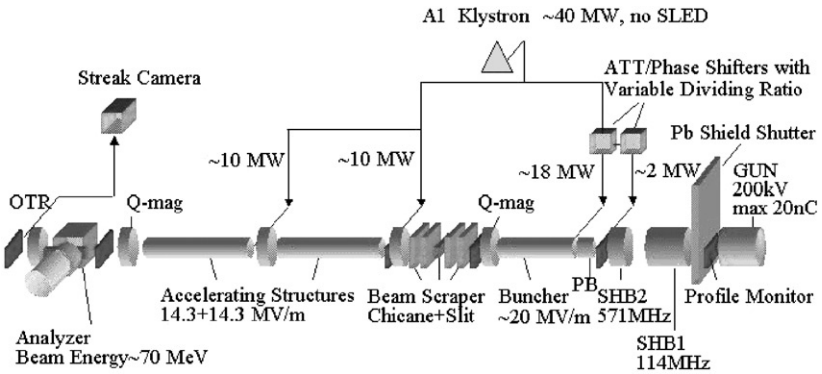

Fig. 2. Profile view of the pre-injector of the linac.

2.1. Pre-injector

The main task concerning the pre-injector (Fig. 2) has been to accomplish a high-intensity, single-bunched beam with a proper beam characteristics: a charge of 10 nC, a bunch length of 4.2 ps (σ: the standard deviation for the Gaussian-curve fit) and a normalized emittance well below

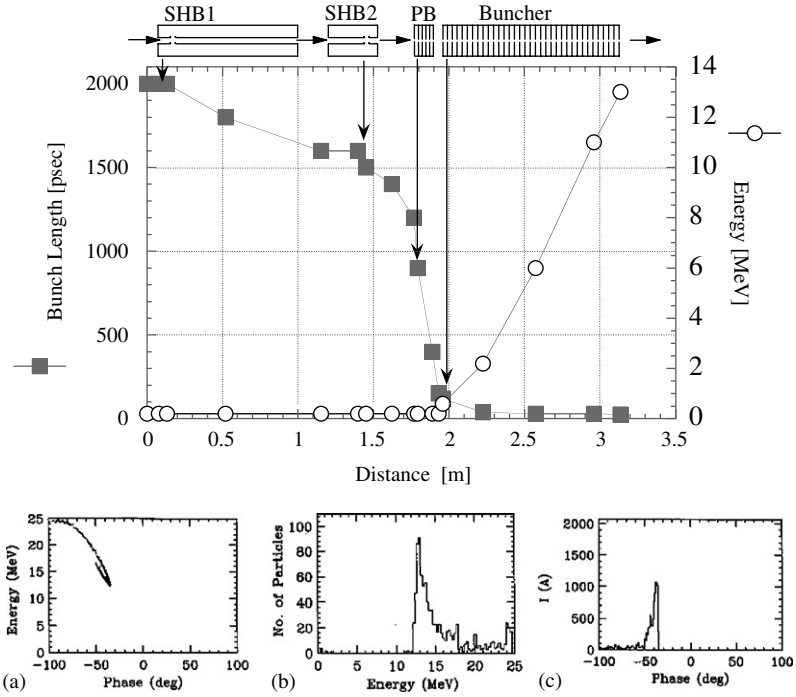

Fig. 3. Simulation of the beam dynamics from a gun to a buncher exit (upper); the beam phase space at the buncher exit (lower).

0.1 mm (σ). The design guidelines for realizing this were the following:

- Increase the pulse voltage of the grid pulser for the electron gun [8] to generate a high-intensity beam, while keeping the pulse length short enough for subsequent bunching sections (2 ns).
- Raise the acceleration voltage (200 kV) of the electron gun so that space-charge forces can be suppressed as much as possible.
- Introduce a two-subharmonic-buncher system [9] (SHB1 at 114 MHz and SHB2 at 571 MHz) immediately after the electron gun, allowing smooth pulse compression in the following bunching section. The principal reason for not adopting a one-subharmonic-buncher system (e.g. SHB2) is that a high-intensity beam with a sufficiently narrow pulse width of 0.6 ns, corresponding to about one-third of the period of SHB2, cannot be generated by the usual grid pulser.
- Restrict the role of SHB1 to gathering all of the electrons from the gun around an appropriate phase range of the next SHB2 by accommodating a relatively modest modulation voltage (100 kV) and a corresponding drift space for rather loose pulse compression.
- Raise the modulation voltage (140 kV) at SHB2 and minimize the subsequent drift space to achieve fast and tight pulse compression against the de-bunching effects due to space-charge forces.
- Integrate the S-band (2856 MHz) prebuncher (PB) and buncher (B) [8] into a single unit to shorten the distance between them for evading any de-bunching effects, while optimizing the acceleration voltage both in PB and B (1.3 MV/m and 20 MV/m, respectively).
- Optimize a solenoid-focusing field in the pre-injector to keep the Brillouin flow for minimizing the emittance increase due to space-charge forces, especially while paying attention to the field strength (maximum 0.2 T) in the first

Table 2
Parameters of the principal components in the pre-injector

Parameters	SHB1	SHB2	Prebuncher	Buncher	Acc. Sec.
Frequency (MHz)	114	571	2856	2856	2856
Shunt impedance (MΩ)	1.14	3.04	14.97[a]	54.50[a]	57.97[a]
Unloaded Q	6989	12580	10140	12000	13810
Power (MW)	0.011	0.007	1	18	10×2

[a] MΩ/m.

several cells at the buncher. Fig. 3 shows simulation results by PARMELA [10], indicating that the designed beam characteristics of a high-intensity, single-bunched beam for positron production is obtained using the parameters listed in Table 2.

2.2. Wake-field issues

The primary concern for wake-field issues was whether a high-intensity, single-bunched primary electron beam for positron production could be stably accelerated up to the positron production target without any degradation of the beam quality due to wake-field effects, which might drastically decrease the positron production yield. In this section, therefore, a discussion is made concerning the single-bunch wake field. Longitudinal wake fields generated at the head particles within a bunch could lead to a large energy spread, which, for instance, might surpass the energy acceptance at the J-arc section. Transverse wake fields caused by an off-axis beam or misalignment of accelerator components might give rise to a head–tail instability, resulting in beam loss or a large beam size on the positron production target. Assuming the parameters listed in Table 3, the wake-field effects have been estimated in a primary electron beam for positron production [7].

The results are summarized as follows:

- The optimum bunch length for a 10-nC beam concerning the energy spread is 1.3 mm (σ). If the bunch length is shorter than this, longitudinal wake-field effects become dominant, giving a larger energy spread compared with the natural energy spread determined by the bunch length.

Table 3
Parameters for investigating the transverse and longitudinal wake fields

Acceleration frequency	2856 MHz
Charge (no. of particles)	10 nC (6×10^{10})
Bunch length (σ)	1.3 mm
Acceleration field	20 MV/m
Total acceleration length	200 m
Initial energy	100 MeV
Final energy at positron target	4 GeV
Betatron wavelength	40 m
Beam size at positron target	0.6 mm
Transverse wake-field strength	3×10^{15} V/C/m^2

- An energy spread of 0.38% (σ) is attained for a 10-nC beam with this bunch length if it is accelerated on an off-crest angle of about 10° in the acceleration phase of microwaves. This is within the energy acceptance of the J-arc section (0.6%).
- According to a numerical simulation for the transverse wake-field effects, the initial offset at the exit of the pre-injector for a 10-nC beam must be much smaller than 0.5 mm, if the beam size on the positron production target is to be 0.6 mm in radius for stable positron production. This could be easily achieved by tuning the corresponding steering coils.
- The same calculation shows that the misalignment of the accelerator sections must be much smaller than 0.8 mm in setting tolerances for a 10-nC beam, while the quadrupole magnets (quads) must be aligned with a precision much better than 0.12 mm. Although the tolerance for the quads might be a rather tight constraint compared to the other, it should be realizable since the best setting error of the present

alignment system so far achieved is around 0.05 mm.
- If the beam charge is larger than the design value of 10 nC, we will need some methods to cure any degradation of the beam quality due to both longitudinal and transverse wake-field effects.

2.3. Beam transport and ECS (energy compression system)

The basic design concepts of the beam-transport system in the linac comprising the J-arc section and the ECS are summarized in the following:

- The beam transport in regular accelerator sections is basically a periodic system of quad-triplets, except for a periodic system of doublets or a FODO system of singlets in some regions where severe constraints on installation space exist.
- The criterion for the optics design is based on the requirements that the 3σ beam emittance, which adiabatically damps with acceleration, should be smaller than the acceptance of the focusing system. The initial normalized emittance at the exit of the bunching section is assumed to be a calculated value (60 μm (σ) by PARMELA), while the acceptance is maximized for a periodic system by choosing an appropriate betatron phase shift in one period.
- Wake-field effects are taken into account for high-intensity, primary electron beams for positron production by installing as many quads as possible along the linac up to the positron production target to strengthen the focusing force.
- In this connection, two different optics are optimized for two modes corresponding to the KEKB electron beam and the positron beam, respectively.
- The J-arc section is designed to be achromatic and isochronous so as to accomplish the conservation of the transverse emittance and the bunch length, assuring preservation of the beam quality [11]. Sextupole magnets are also introduced for higher order corrections.
- The ECS comprising a chicane-magnet system and two accelerator sections is introduced into the end of the linac for almost halving the large energy spread of positron beams ($\sigma_{\text{design}} = 0.25\%$), which is about twice as large as that of the beam-transport line to the ring ($\sigma_{\text{design}} = 0.13\%$).

Optics simulation results by TRANSPORT [12] are shown in Fig. 4, verifying that the calculated beam size is well below the physical aperture.

3. Main accelerator module

The basic composition of the main accelerator module involves four 2-m accelerator sections fed by one high-power klystron. The standard module length is 9.6 m. Each module has an energy gain of 160 MeV with a klystron peak power of 41 MW and using a SLED-type rf pulse compressor. A total of 55 modules can therefore accelerate electrons to a maximum energy of 8.8 GeV.

These modules are installed in an underground accelerator tunnel, and are connected to the rf source in the klystron gallery at the ground level. The two rooms are separated by a 2.5 m thick concrete wall for radiation shielding (Fig. 5).

3.1. Accelerator structure

The accelerator section is an S-band (2856 MHz), 2 m long disk-loaded structure of the $2/3\pi$ mode (Fig. 6). The structure was designed to produce a quasi-constant axial electric field by changing the disk-hole diameter (the so-called 2a dimension) stepwise by 75 μm from the entrance to the exit over the 2-m section. For dispersing the resonance frequency of beam-blowup modes, though this effect concerns the multi-bunch case, six types of structures were made with different sets of 2a dimensions. The shunt impedance of the structures is from 57.3 to 58.3 MΩ/m and the filling time is 0.46 to 0.56 μs.

All of the structure were fabricated by an electroplating technique, which is used to form

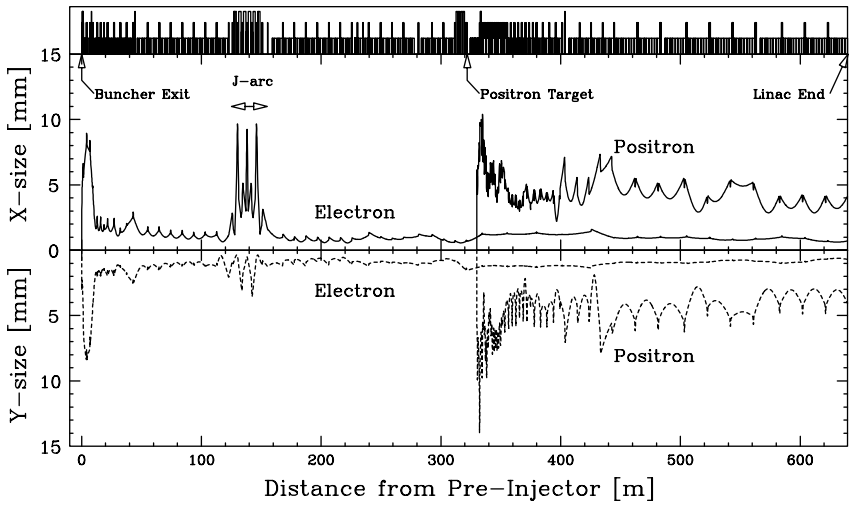

Fig. 4. Calculated beam profiles through the linac. 8-GeV electron beam profile along the entire length of the linac; (solid line) horizontal; (dashed line) vertical. 3.5-GeV positron beam profiles downstream from the positron production target; (solid line) horizontal; (dashed line) vertical.

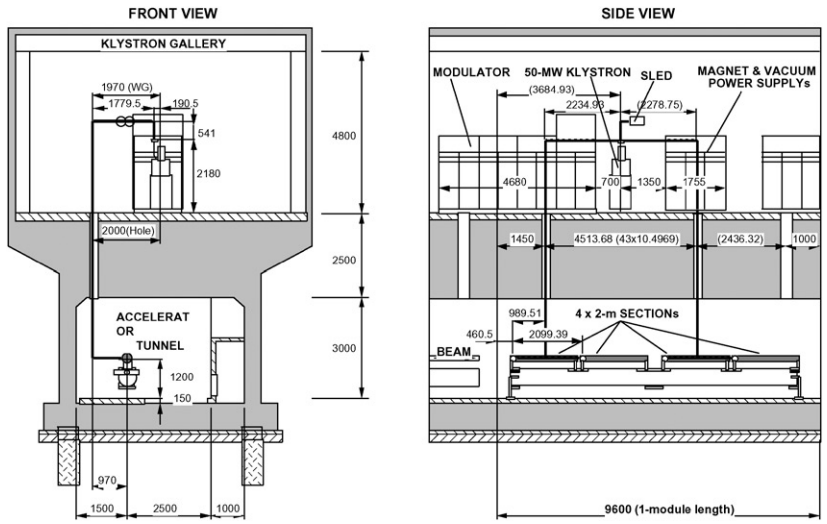

Fig. 5. Cross section of the linac main module.

an integral, vacuum-tight structure by electroplating the outside of an assembly made of disks and cylinders. The thickness of the electroplating is 5 mm. An advantage of this method is to eliminate the need for tuning, because the electroplating is made in a room temperature and hardly distorts the precisely machined dimensions. About eighty sections were newly fabricated for the extension of the linac [13].

Before the upgrading, using a resonant ring, one of the old accelerator sections fabricated during 1980–1981 was tested to assure that it could operate at more than 20 MV/m [14]. After having fabricated a new rf source, the new accelerator section was conditioned for an accelerating field of up to 40 MV/m [15].

The operation temperature is 30°C, which is maintained within 0.1° so that the phase shift

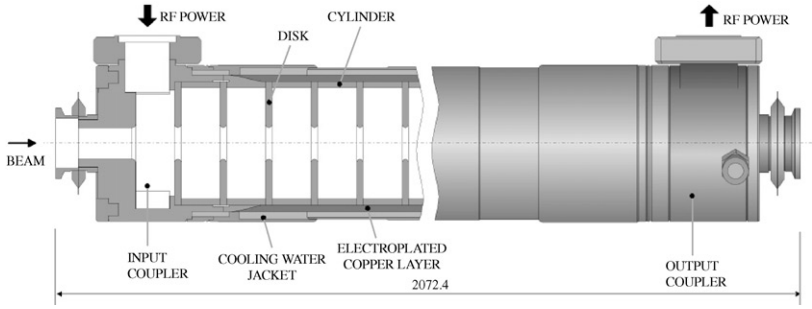

Fig. 6. Cross section of the 2-m section used in the main modules.

along the entire length of an accelerator section is kept within 2°.

The vacuum system for the old injector was used for the main modules, with improvements in some locations such as rf windows separating klystrons from accelerators and the positron capture sections. The vacuum inside the regular accelerator sections is estimated to be several 10^{-6} Pa by using a pressure-distribution analysis method [16].

3.2. Alignment of the module

As described in the previous section, the linac modules must be aligned along the straight beamlines with a precision of better than 0.8 mm in accelerator structures and 0.12 mm in quadrupole magnets. The alignment was conducted in the following way:

- Four accelerator sections, assembled with waveguides and vacuum pipes, are pre-aligned on an 8-m steel girder, which are to be connected to an rf source after being installed in the beamline.
- The modules are moved to the beamline by a special electric transport system.
- Laser beamlines are preset 420 mm below the accelerator beamline.
- The accelerator modules are aligned in reference to the laser line by using quadrant semiconductor detectors mounted on both ends of the girder [17].

To facilitate horizontal positioning of heavy and rigid bodies, the girder is supported using ball bearings. For vertical smoothness, the waveguides are supported utilizing spring balances.

4. Rf system

The rf system was upgraded for KEKB. The entire rf system consists of a main-drive system, eight sub-drive systems with two stand-alone rf drivers for the pre-injector and a positron-capture section, and 59 high-power pulsed klystrons with modulators. A block diagram is shown in Fig. 7.

4.1. The drive system

The master frequency of the linac was 571.2 MHz; this is the 5th subharmonic of the linac fundamental frequency, and is also used for SHB2. The main drive system [18] was newly equipped with a frequency multiplier/divider which generates the linac fundamental frequency (2856 MHz) and the linac-ring common frequency (10.385 MHz); using this, necessary reference signals for SHB1 (114.24 MHz) and for the KEKB ring (508.9 MHz) are produced. The multiplier/divider was manufactured so as to have a very low noise performance in order to minimize any rf phase jitter.

Eight sub-boosters, each of which drives four or eight high-power klystrons, were reinforced to generate 60-kW rf pulses [19].

Solid-state 10-kW amplifiers were newly installed for the 114-MHz and 571-MHz subharmonic bunchers.

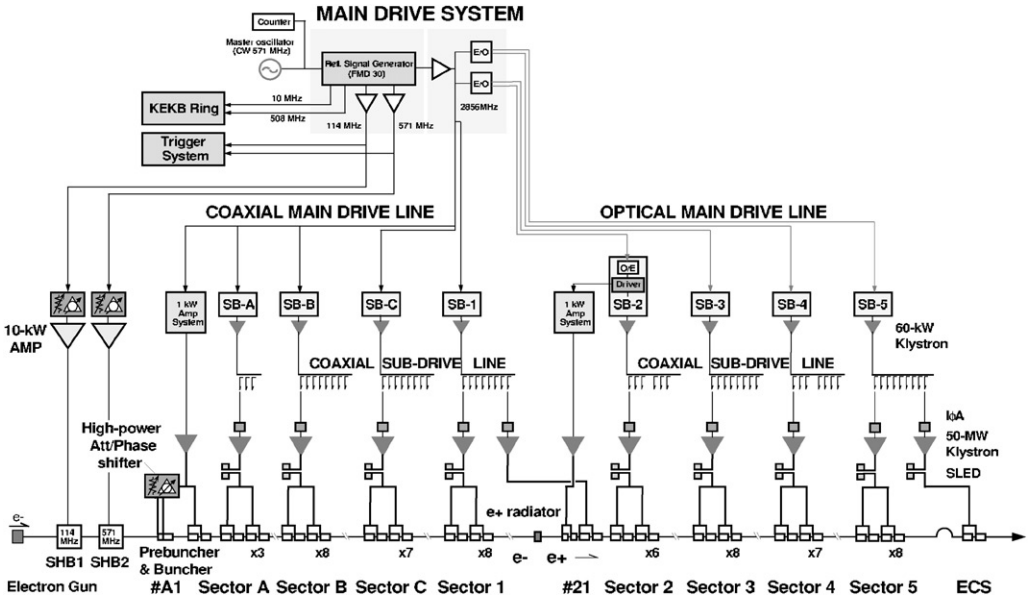

Fig. 7. General block diagram of the entire rf system.

A feedback controller was installed in every klystron-drive circuit to stabilize the phase and amplitude of the cw-rf signal; this stabilized signal was monitored and used as a phase reference [20].

4.2. General concepts for upgrading the high-power rf system

An upgrade of the linac rf power was achieved by combining a power increase of individual klystrons and SLAC-type rf compressors (SLED). In upgrading the linac, the existing components of the 2.5-GeV linac rf system [21] were utilized as much as possible in order to save construction time and cost.

Regarding the rf source, it was decided that the one-pulse energy from the modulator should be doubled so that the capacitance of the pulse forming network (PFN) capacitors in a modulator would be doubled at the same charging voltage. In this way it was possible to reuse many rf components. By doubling the capacitance and obtaining an output-pulse width of 4 μs, most of the main parameters of the rf system can be automatically determined. In these schemes the required electron energy (8 GeV) is achieved along with an appropriate number of standby tubes [22].

4.3. Modulator

The modulator for the 2.5-GeV old linac had been successfully operated without any serious problems [23]. A two-times increase in the PFN capacitors at the same charging voltage required a new IVR, a rectified transformer, a filter choke and a charging choke, while rectifier diodes and hold-off diodes did not need to be changed by adopting water cooling. In the PFN, two circuits with 20 capacitors (0.0147 μF) and 20 inductors (0.33 μH) each were placed in parallel. In this arrangement, smooth flat-top pulses were obtained [24]. The thyratron was also changed with ITT F-241s. Due to these modifications, the modulator cabinet of the pulse circuit section was reinforced to be larger.

4.4. Klystron and its assembly

From the requirement that any modification of the rf system must be conducted during an interval of machine operation for the PF experiments, minimum changes to the existing system were desirable. In accordance with a FCI [25] simulation of the previous 30-MW klystrons, producing a 50-MW output power from the

30-MW klystron succeeded with modified high-voltage insulation.

For more stable operation, a new 50-MW klystron having the same interaction region and collector was developed as follows. The cathode and the gun geometry were improved for higher voltage operation, but the same focusing magnet could possibly be used with slight modifications. At the same time, the pulse transformer was rewound to a step-up ratio of 1:13.5 from the previous one of 1:12. A heater transformer and a high-voltage insulator were newly developed in order to use the old klystron oil tank. Therefore, we could use the same-size klystron assembly even though the output power was increased from 30 to 50 MW [26].

This klystron could output more than 60 MW for the buncher and positron source sections under the operational condition of a shorter pulse width. The klystron output characteristics are shown in Fig. 8. This klystron used the BI-cathode; it has been running with a sufficient lifetime [27]. This tube had a single output rf window using high-density pure alumina of 99.7% with a thin TiN (or TiON) film to prevent arcing on the window [28].

4.5. SLED

The SLED cavity for KEKB was manufactured based on one of JLC-ATF with a dual-wall coupling iris (TE015 mode, $Q = 100,000$) [29]. This gave a theoretical energy multiplication factor of 2.01 maximum and 6.4 for the coupling coefficient between the waveguide and the cavity. However, 1.95 was obtained for the multiplication factor when the rise time of the rf pulse was 100 ns and the phase reversing time was 200 ns [30]. A schematic diagram was shown in Fig. 9.

The entire picture of the modulator, the klystron assembly and the SLED cavity is shown in Fig. 10.

4.6. Rf operation status

The operation of the upgraded rf system was started in 1998. The full rf system has been successfully operated. In order to operate the linac stably, various monitoring systems were also upgraded for this project.

Rf monitoring systems for power level and phase were installed in all high-power klystron modulators and are controlled with a VXI-based controller. These enable us to diagnose effectively operational problems relating to rf sources. The stability of the master oscillator is also monitored.

Each klystron modulator is controlled with a PLC-based controller, which monitors interlock status and vacuum status, and also presents the historical record of the operation data. During operation, the average rf fault rates due to the VSWR interlock, which trips over the limiting value of 1.4 to protect the rf window from failure, are about 2–3 times/h/59 klystrons and operations are automatically restarted after 5 s. When an accelerator section causes frequent breakdowns, it is re-processed by utilizing an "auto aging program", installed in the PLC controller, during the idling interval between the beam injections.

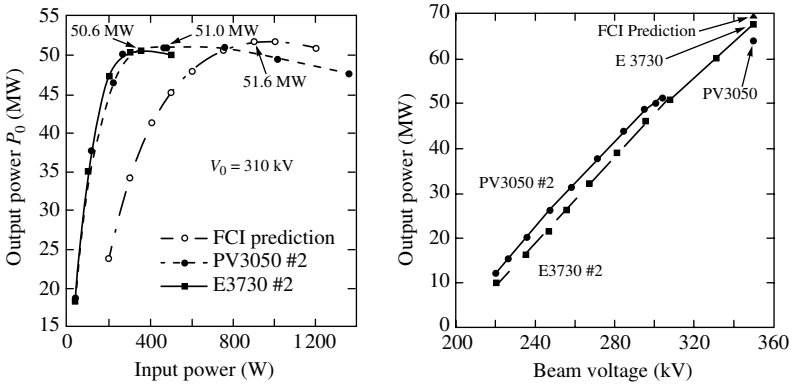

Fig. 8. Klystron output characteristics.

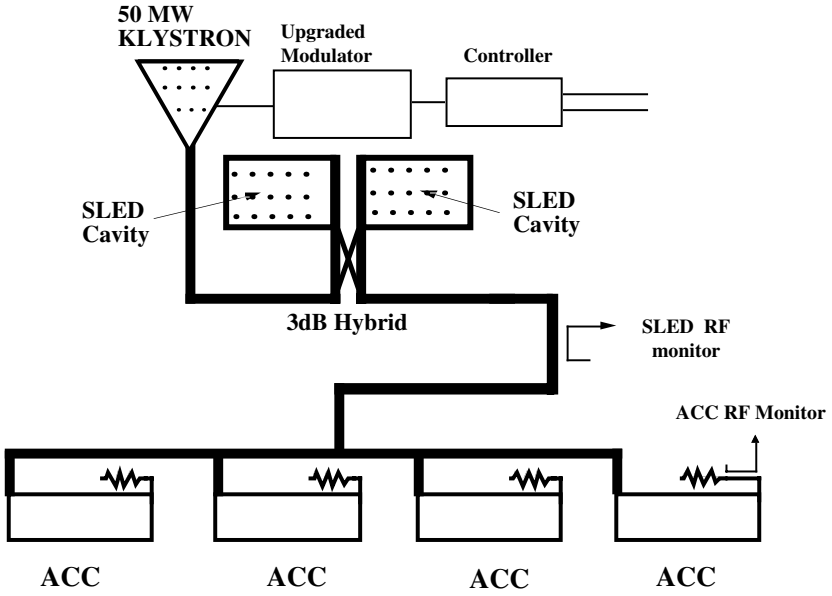

Fig. 9. Schematic diagram of the rf pulse compressor.

Fig. 10. The entire picture of the modulator, the klystron assembly and the SLED cavity.

5. Trigger system

The trigger system is connected with the rf drive system and is constructed to provide synchronization between the ring and linac rfs. They must be synchronized so as to meet the requirement for injection precision (+/− several-tens of picoseconds) [31].

The master beam timing-signal, which is the synchronized frequency between the linac-rf and ring-revolution frequencies, is obtained by dividing the common frequency (10.385 MHz) by the ring harmonic number (5120). The ring rf-bucket can be selected by delaying the master timing-signal in units of the common clock (10.385 MHz). The gun-beam triggers are then generated by synchronizing the master timing-signal with the linac pulse repetition signal (50 Hz at the maximum).

The trigger signals are transmitted along the linac by superposing them on 571-MHz rf signals. They are distributed to more than a 100 local pulse-drive systems, not only the electron gun but also other systems such as rf pulse modulators and beam monitors. Received trigger signals are shaped and re-synchronized with the 571-MHz rf signals.

6. Electron pre-injector

The pre-injector consists of an electron gun, a bunching system and two regular accelerating sections. The bunching system is composed of

two sub-harmonic bunchers (SHBs) with frequencies set at the 25th and 5th subharmonics of 2856 MHz, and a prebuncher (PB) and a buncher (B) at 2856 MHz. As described in the previous section, the pre-injector has a function which makes the gun pulse to be a tight single bunch capable of being accelerated in the following regular accelerator sections at 2856 MHz [32]. Its operation parameters are listed in Table 2. The main features of the components are as follows.

6.1. Electron gun

The requirements for the gun are a 200 kV accelerating voltage and 15 nC maximum charge for a pulse width of less than 1 ns. A triode-type thermionic gun with a dispenser cathode of 2 cm^2 (Fig. 11) and a high-speed grid pulser are employed for such a high current. It has a superb pulse feature of small time jitters ($\sigma = 4$ ps) as well as short pulse lengths. It also has an electric analogue time-delay module that continuously varies the gun trigger timing over a 3-ns range [8]. This function is used for a digital feedback system to stabilize the beam timing. The grid pulser also controls the beam repetition (maximum 50 Hz) with external trigger signals, as well as the beam intensity (1.2 and 12 nC) by changing the output voltage.

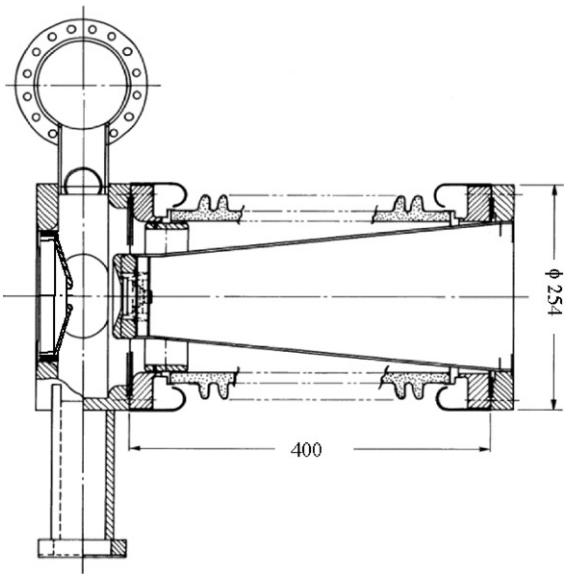

Fig. 11. Electron gun.

6.2. Subharmonic bunchers

The SHB frequencies are chosen from subharmonics near 100 and 500 MHz with the condition that each frequency should be a multiple of the linac/ring common frequency of 10.385 MHz, which is a $5 \times 5 \times 11$th sub-harmonic of 2856 MHz, resulting in the 25th and 5th subharmonics.

The first SHB operating at 114.24 MHz (25th subharmonic) and the second SHB at 571.2 MHz (5th subharmonic) are both a standing-wave type re-entrant cavity with a tuning knob [9]. The dimensions are given in Figs. 12a and b. The rfs are fed by corresponding 10-kW solid-state amplifiers through coaxial cables.

6.3. Prebuncher and the main buncher

The prebuncher and the main buncher are both traveling-wave type disk-loaded waveguides in which the phase shift is $2\pi/3$ per cell (Fig. 13). Since the gun beam is to be velocity-modulated at around $\beta = 0.7$, all of the cell lengths are $\beta\lambda/3$ in the prebuncher, where β is the velocity in units of the light velocity, and λ is the free-space wavelength of the accelerating rf (10.5 cm). In the main buncher, however, the cell length varies from $\beta\lambda/3$ to $\lambda/3$ during the first 6 cells, because the gun beam has to be accelerated to form a tight bunch as well as be modulated in velocity.

As shown in the figure, the KEK prebuncher and the main buncher are assembled into one united body in order to reduce the distance between them and to suppress the divergence due to a strong space-charge force [33]. The number of cells is four in the prebuncher; although that in the buncher is 33, bunching occurs through only the first few cells and the β of the beam reaches almost unity.

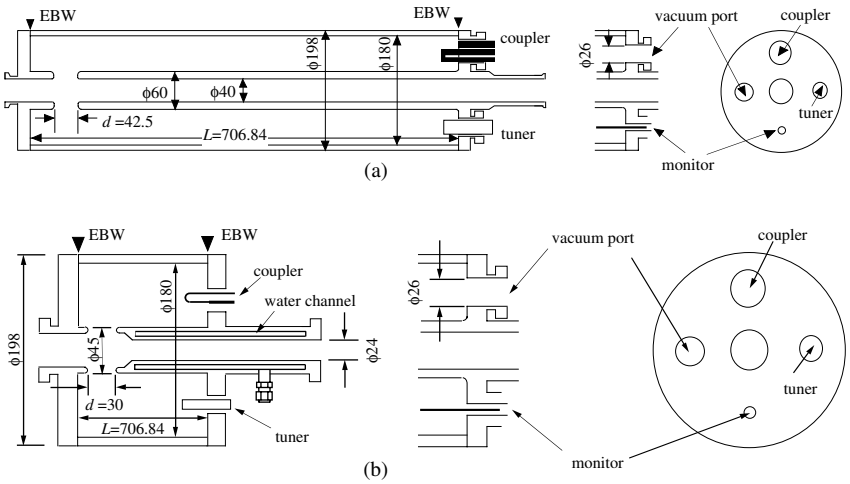

Fig. 12. SHB1 and SHB2.

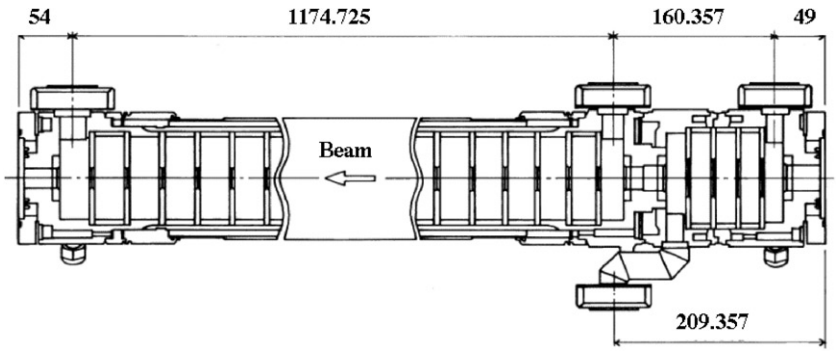

Fig. 13. Prebuncher and buncher.

6.4. The rf power dividing system for the pre-injector

The waveguide system comprises rectangular waveguides, power dividers, phase-shifters and attenuators, which are operated in a vacuum (Fig. 14). Typical powers fed into the buncher sections are 2 MW (prebuncher), 18 MW (buncher), 10 MW × 2 (two regular sections). The phase-shifter and attenuator were improved so that the power dividing ratio between the prebuncher and the buncher and their phases can be varied independently [34]; this function has made it much easier to adjust the buncher sections.

6.5. Stabilizing the pre-injector

For stable operation, the bunch timing or phase with respect to the accelerating rf wave must be fixed as well as the bunch shape. If the status of the gun and the bunching section would become unstable, the bunch timing and shape would be changed. The tolerances for the devices are severe in the case of a high-intensity beam of 10 nC, as are shown in Table 4. The stability in the operation meets the requirements owing to digital feedback loops [35]. The tolerances on the devices came from the goal of keeping the beam transmission rate above 90% at the target.

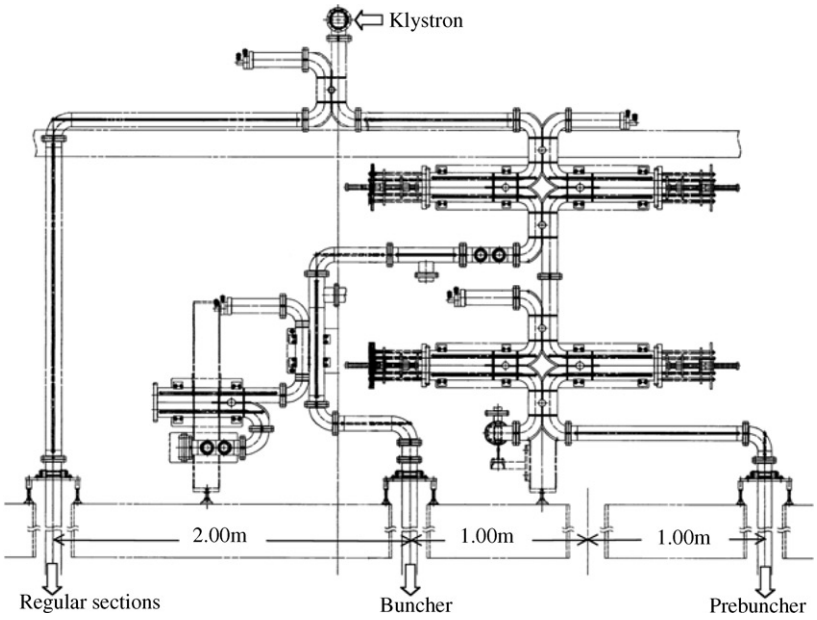

Fig. 14. Power-dividing system.

Table 4
Tolerance to stabilize a high-current beam

Beam timing	±45 ps
Gun high voltage	±0.38%
SHB1 phase	±1.1°
SHB2 phase	±1.3°
Buncher phase	±1.7°

7. Positron source

The KEKB positron source comprises a positron production target, a strong pulsed solenoid, two 1-m accelerator sections, two 2-m accelerator sections, long DC solenoids to cover all these capture sections, and a positron/electron separator (Fig. 15).

The positron production target is a water-cooled 14-mm (4 radiation-length) tungsten plate, which is able to be inserted into the beamline when a positron beam is needed. Since the primary-beam power to hit the target became as high as 1.9 kW by upgrading the positron intensity, this target was newly developed. To relax the heat stress and to maintain heat contact with the cooling channel, a tungsten–copper functionally graded material is used for the target.

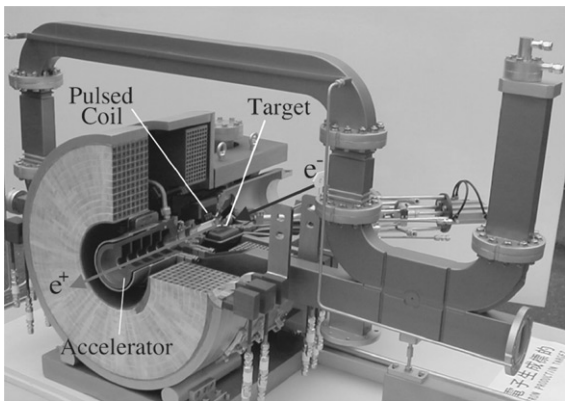

Fig. 15. Positron source.

Positrons emerging from the target are focused sequentially by two types of solenoidal magnetic fields. The first one is a short, strong field of 2 T produced by a 45-mm long pulsed coil [36] (the so-called quarter-wave transformer). The pulsed

current (10 kA at 2 kV) is provided by a solid-state power supply. The second is an 8-m long, 0.4-T produced field by a DC solenoid. The positron yield and its normalized emittance are determined by the solenoid focusing system acceptance (5.9 mm).

Captured positrons are accelerated by the following four accelerating sections covered with the 8-m DC solenoid. The first 1-m section has a two-iris input coupler and large aperture disks. This structure was adopted so as to avoid any discharge in the strong magnetic field and strong radioactivity, which might degrade its performance.

The positron/electron separator accommodates a chicane composed of four rectangular magnets and a beam stopper at the center of the chicane. In the KEK positron source, the rf phase is set so that captured positrons are accelerated from the beginning of the first capture section (the so-called positron acceleration mode); consequently pair-created electrons are first decelerated, but the phase slips by 180° when the electron speed decreases below the light velocity, and they again come to be accelerated. Even in the case of an inverse phase preset (positron deceleration mode), the situation that both positrons and electrons which emerge from the target are accelerated is not changed. Thus, the separator is essential to cut the electrons and to clearly observe the signals for adjusting the positron beam.

8. Beam instrumentation

The beam instrumentation in the linac was much improved in order to enable operation of a high-intensity, high-stability beam for the KEKB rings. Especially, beam diagnosis to monitor and suppress transverse and longitudinal emittance growth was most important. According to a wake-field simulation, a beam with a charge of 10 nC/bunch should be guided within transverse positions of 0.12 mm along the center of the quads. Thus installation of beam-position monitors inside the quads was essential.

Table 5 is a list of beam monitors installed in the linac.

Table 5
Beam monitors at linac

Type	Purpose	No.
Streak camera	Bunch length	4
Beam position monitor	Beam position/charge	90
Wall current monitor	Beam charge	68
Screen monitor	Beam emittance/energy-spread	112
Wire scanner	Beam emittance/energy-spread	14

8.1. Streak camera

It is important to measure the longitudinal and transverse beam profiles at the bunching section of the linac, since they define most of the beam characteristics. A streak-camera system was employed to measure the longitudinal beam-bunch profile.

Optical transition radiation produced from a polished stainless-steel plate (SUS304) is lead through an optical transport system without any distortion to a streak camera with a time resolution of 2 ps. The controls of the camera read-out, image analysis, timing and optical systems are integrated into an application program to ease routine measurements [37].

Systems with the same configuration were installed at three other locations (just after the J-arc section, the positron-capture section and the ECS section) in order to diagnose an isochronous condition, optimum positron generation parameters and the ECS performance, respectively (Fig. 16).

8.2. Beam-position monitor

High-current primary electron beams are required for a sufficient amount of positrons, while the beam orbit must be controlled so as to suppress any beam blow-up generated by the large transverse wake fields. Thus, a stripline-type beam-position-monitor (BPM) system was newly developed with a resolution of less than 0.1 mm (Fig. 17).

Along the linac, 90 stripline-type BPMs have been attached to the pole pieces of the quadrupole magnets. The response functions of each BPM using third-order polynomials were determined at

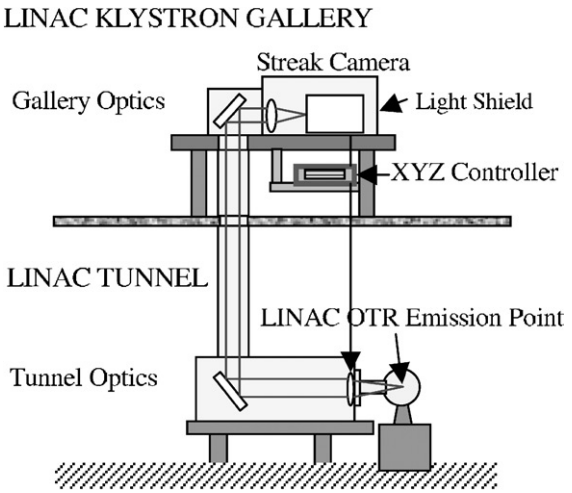

Fig. 16. Streak-camera system installed at the pre-injector.

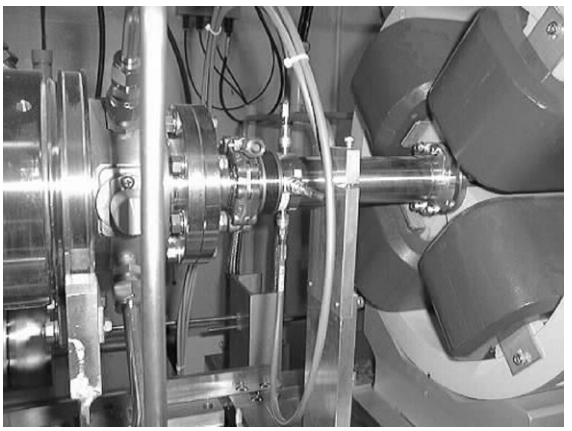

Fig. 17. Installed beam-position monitor.

a test bench before installation. The beam-based calibration was also applied with electron beams after installation. The beam charge was calibrated using a Faraday cup with electron beams. The beam position offset against the quadrupole magnet center was determined by varying the strengths of an upstream steering magnet and the quadrupole magnet [38].

Four signals from a BPM are connected with one of 18 measurement stations through doubly shielded cables. At each station, those signals are delayed by appropriate delay-lines so as not to overlap each other, and are fed into waveform

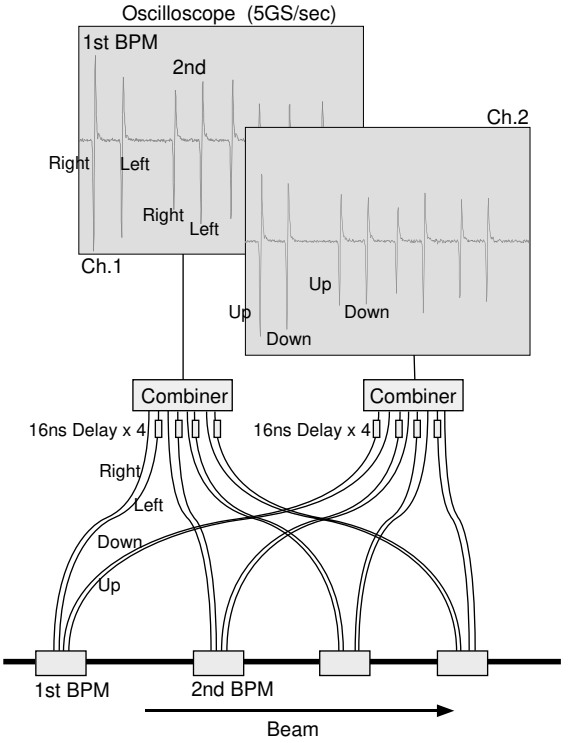

Fig. 18. Block diagram of the beam-position monitor system.

digitizers of 5 Gs/s. The waveform is read through the GPIB and analyzed with predetermined calibration factors once per second by a VME computer. Since the timing and amplitude ranges are dependent on the beam modes, the process is driven by a control database system [39].

Acquired beam positions are sent to central computers and used by various beam-feedback systems to maintain stable beam operation [40] (Fig. 18).

8.3. Wall-current monitor

Wall-current monitors have been used to measure the beam charge [41]. They were useful to ensure the calibration factors of the BPMs described above. Each monitor is equipped with four electrodes around it; the signals are combined to eliminate any beam-position dependence. At some locations where the BPMs are not installed, four signals are read independently to measure the beam position (Fig. 19).

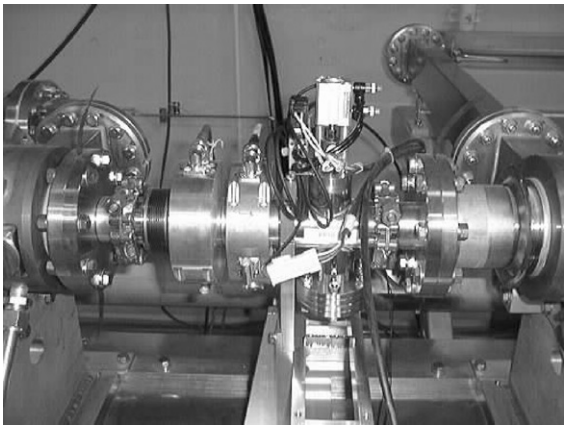

Fig. 19. Wall-current monitor (left) and a screen monitor (right).

8.4. Screen monitor

Screen monitors were installed in order to observe the transverse beam profile. A compact-type monitor was newly developed to leave space for other beam-line components. Screen material (Al_2O_3 (99.5%) and CrO_3 (0.5%)) with a thickness of 1 mm was chosen so as to obtain a sufficient amount of fluorescent light. The screen is driven by a pneumatic actuator and controlled by a VME computer. The beam image is viewed by a CCD camera and is sent to the central console room through video signal selectors.

At about ten locations where the transverse emittance or the energy spread should be precisely measured, random-shutter cameras and 0.1-mm-thick screens instead of standard ones are employed. Twiss parameters are derived from beam-size measurements, while varying the upstream quadrupole magnets (Q-scan method).

8.5. Wire scanner

Transverse emittance measurements and matching should be managed in order to transport beams. In order to carry out the tasks non-destructively, wire scanners with sufficient betatron phase separations were installed. Three groups of four wire scanners were installed before and after the J-arc section and at the end of the linac, respectively [42]. Each wire scanner is equipped with three tungsten wires of 0.1 mm diameter to measure the horizontal and vertical beam distributions and their coupling. Bremsstrahlung emitted from a wire by an electron beam is detected by a downstream photomultiplier tube (Fig. 20).

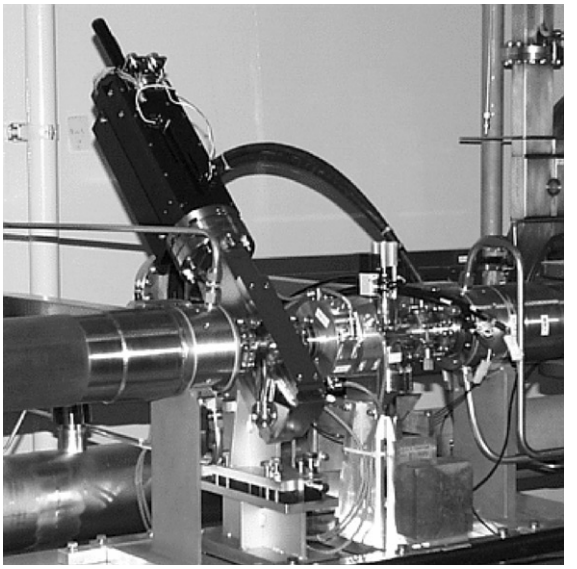

Fig. 20. Wire scanner installed on the beam line.

A software panel was developed to automate the measurements and beam-optics calculations. The twiss parameters are measured daily and optics matching is carried out using upstream quadrupole magnets if the matching condition is not optimal.

An independent wire scanner was installed inside the J-arc section, where the dispersion is large, to measure the beam-energy distribution. Another wire scanner was also installed just after the bunching section to measure the emittance using the Q-scan method.

9. Control system

The linac control system was rejuvenated in 1993 and has been improved continuously [43,44]. The base of the control system comprises UNIX

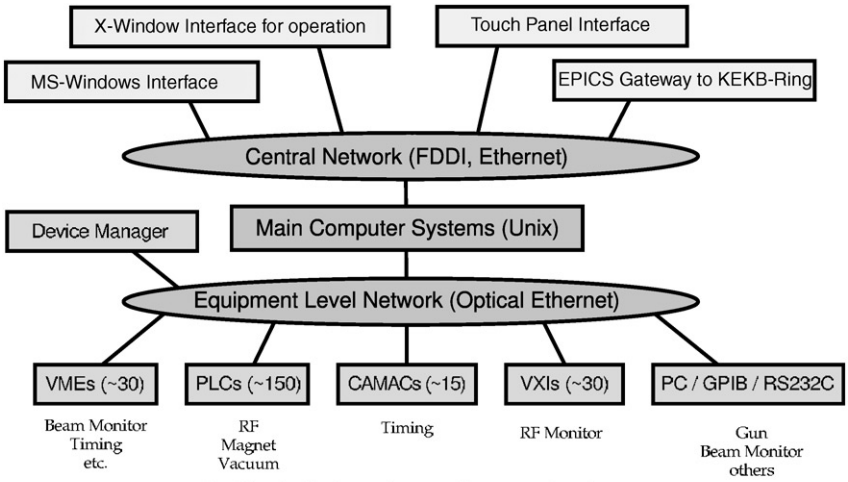

(a) Physical view of control system hardware.

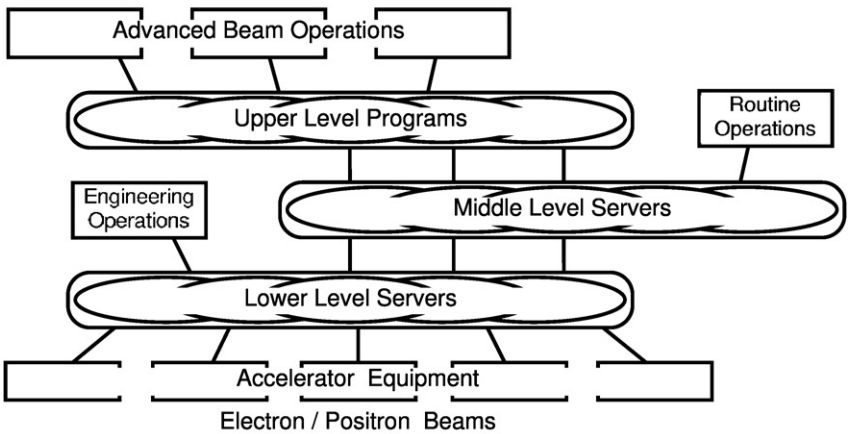

(b) Logical view of control system processes.

Fig. 21. Block diagrams of the control system architecture.

computers and local device controllers. The home-made remote procedure call (RPC), based on the TCP and/or UDP protocols, are used for communication between them. The overall views are shown in Figs. 21(a) and (b).

9.1. Control architecture

As shown in Fig. 21(b), there are three software layers in the control scheme. The lower-layer services correspond to different types of control hardware, such as 16-bit binary outputs in VME computers. They represent hardware details including error recoveries, which should be hidden from the upper layers.

The middle-layer controls are served by central Unix computers, which represent the abstract behaviors of the accelerator equipment, such as power supplies. One middle-layer service may utilize several lower-layer ones.

The upper-layer application programs carry out actual linac operations utilizing as many middle-layer services as they need. By using the network RPC scheme, upper-layer application programs can be executed by any computers on the control network, although a security measure is applied.

Several gateway programs were developed on top of middle-layer services, in order to exchange the linac information with other environments. Those include a portable channel access server for the EPICS control environment at the KEKB ring [45] and a CORBA interface for archived data retrieval [46].

9.2. Device controllers

While we had many old controllers which are about 20 years old, every year new technologies are revealed. During the KEKB project, we have replaced the old controllers with new ones. The newly introduced controllers utilize VME, VXI, CAMAC, PC and PLC (programmable logic controller) technologies, depending on the needs specific to the corresponding accelerator equipment. Many of the controllers employ PLCs, which are directly connected to network, if the requirement for processing speed is not critical [47].

9.3. Central computer and network

An Unix cluster server and 2–4 Unix computers carry out most of the middle- and upper-layer control tasks. The cluster server system realizes a fault-tolerant operation over several months.

The computer network for controls comprises an FDDI backbone (100 Mbps) and many Ethernet segments (10 Mbps), which are linked together with a star-like topology in order to localize any problems. The connections to local device controllers are based on the 10Base-FL Ethernet (fiber-optic cables), which is essential to eliminate electro-magnetic noises from the high-power klystron modulators in pulsed operation. Important 10Base-FL segments have redundant links for fault-tolerant network operation. While the number of fiber-optic connections are more than 200, the number of failures is less than 10 per year, some of which are automatically recovered by redundant links.

Besides running control-process software, Unix computers also support many general network services, such as file services, name resolutions, remote booting, time synchronization, world-wide-web, printer and mail services. They are important to exchange information quickly between equipment experts, the control group and the commissioning group.

PCs running Windows operating systems are also employed for operator consoles [48,49]. They provide various linac status displays and interfaces to electronic log books.

9.4. Commissioning software

For the linac commissioning, the following application-software environments are used: (a) the Tcl/Tk programming language for simple operations, and (b) the SADscript [50] for advanced beam operations and studies. Both of them have interfaces to the control system and the Tk graphical widgets on X-window. Many common routines are provided as libraries, such as control-system RPC interfaces, graphical user interfaces, operation procedures with error recovery, parameter save/restore, debugging facilities, and inter-application communication [51].

There are more than one hundred application programs registered in the linac commissioning software launcher, which have been updated frequently to meet the requirements in the commissioning [52]. They include a beam-mode switcher, beam-energy and beam-orbit feedback systems, an emittance measurement and matching system, and an adaptive beam-orbit correction program [40]. They all run online with graphical user interfaces, thus greatly ease the commissioning.

10. Beam commissioning and operation

10.1. Commissioning

Beam commissioning has proceeded step by step since the autumn of 1997, continuing the construction of the remaining parts as well as the ordinary injection into the Photon Factory rings (PF), even during the linac upgrade. The design goal was fully achieved in spring, 1999, just before the detector (Belle) roll-in at the interaction point

of the KEKB rings. The main achievements so far established are the following [54]:

- Fine-tuning of the pre-injector has brought about quite good performance concerning a high-intensity primary electron beam for positron production as well as a low-intensity electron beam for direct injection to the KEKB ring. A 10-nC beam with a bunch length of 4.2 ps (σ) and a 1-nC beam with that of

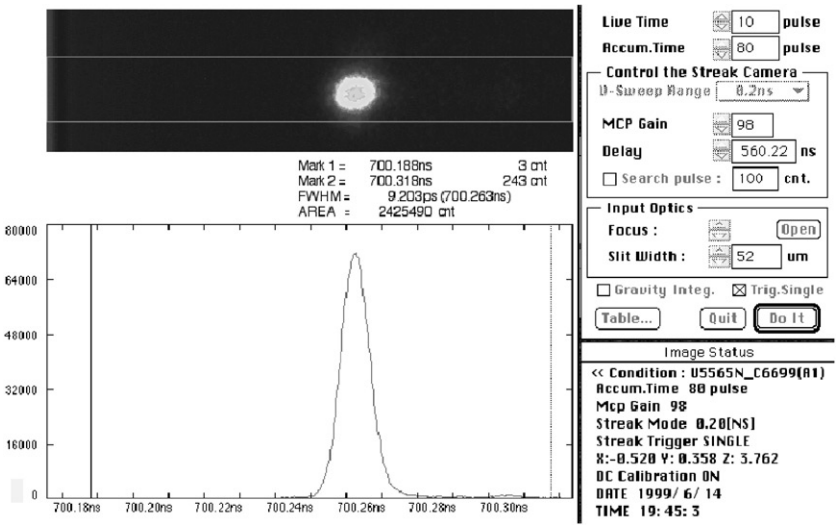

Fig. 22. Longitudinal profile of the 10-nC bunch observed with a streak camera.

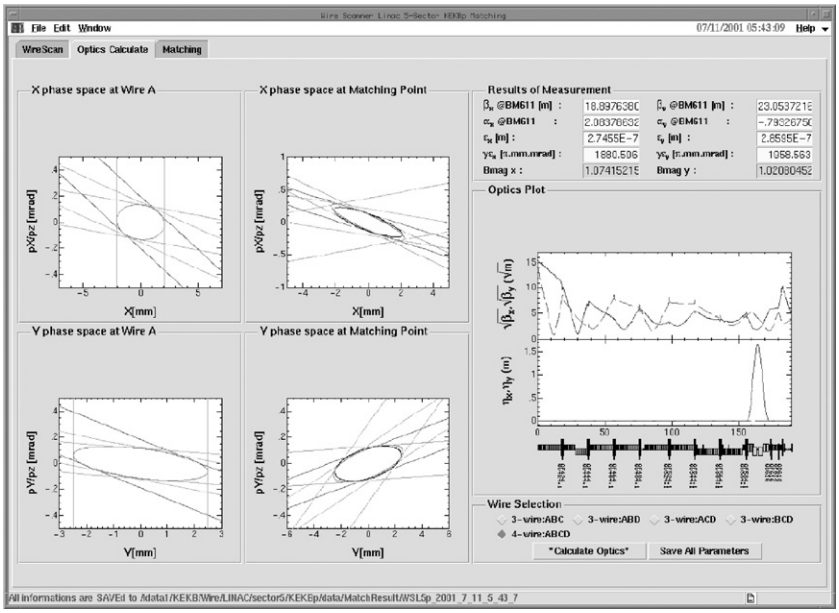

Fig. 23. Optical matching results in the linac.

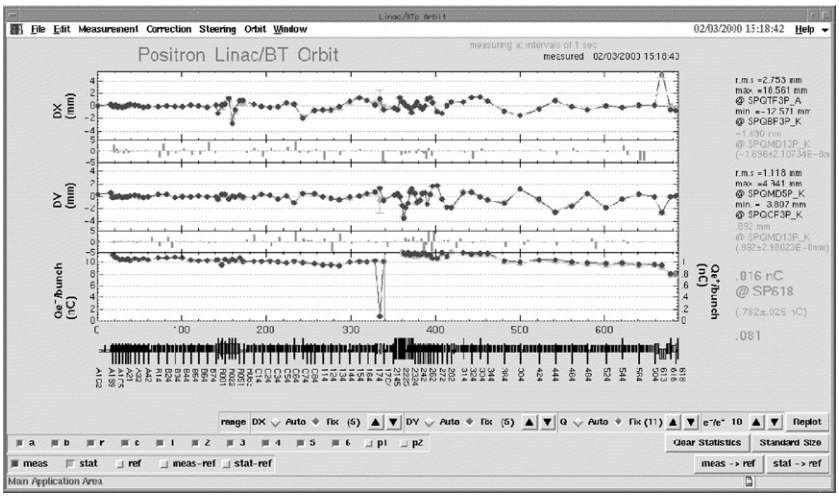

Fig. 24. Beam orbit display along the entire linac length.

2.5 ps (σ) have been obtained at the end of the pre-injector with a quite good stability regarding the charge intensity and timing, ensuring stable acceleration in the following accelerator sections (Fig. 22) [8].

- The optics along the whole linac was checked by measuring the twiss parameters with wire scanner monitors installed in several locations in the linac [42]. Optics matching, especially at the end of the pre-injector, in the J-arc section, at the end of the positron-capture section and at the end of the linac (Fig. 23) has been intensively carried out, giving satisfactory results [55].
- The beam orbit from the electron gun to the end of the linac (Fig. 24) has been controlled with an automatic orbit-correction program, while avoiding in particular any beam blowup due to transverse wake fields caused by beam offsets.
- The energy spread of positron beams ($\sigma_{\text{meas}} = 0.30\%$) has been compressed into a half width through the ECS ($\sigma_{\text{meas}} = 0.15\%$), reaching almost the energy acceptance of the ring injection line ($\sigma_{\text{design}} = 0.13\%$) (Fig. 25). The ECS also suppresses any energy variation upstream, thus improving the energy stability.

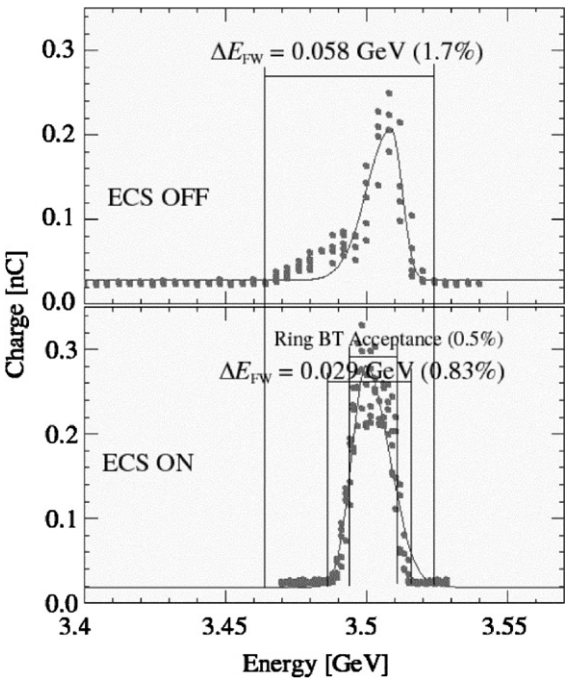

Fig. 25. Energy width at the end of the linac.

10.2. Operation

Since May, 1999, when Belle started to accumulate the integrated luminosity for CP-violation

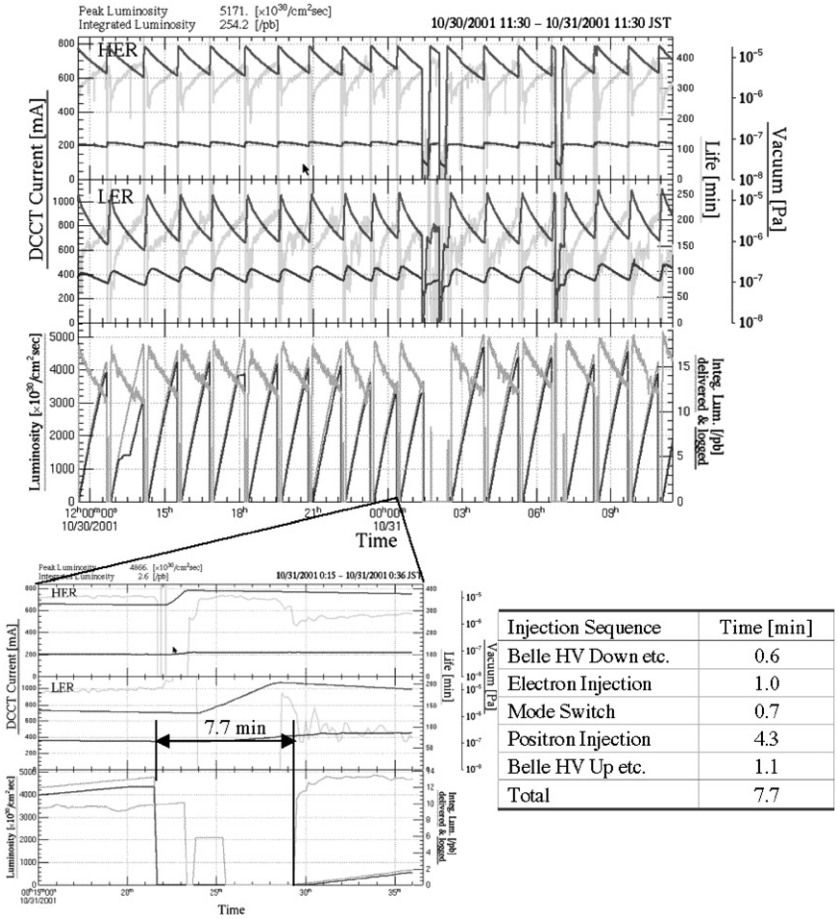

Injection Sequence	Time [min]
Belle HV Down etc.	0.6
Electron Injection	1.0
Mode Switch	0.7
Positron Injection	4.3
Belle HV Up etc.	1.1
Total	7.7

Fig. 26. Accumulation of the integrated luminosity.

measurements, the KEKB linac has been operated without any big problems concerning injection, which could cause a long loss time for the accumulation of the integrated luminosity (Fig. 26). The beam mode switching [40] among four different beams for the two KEKB rings (positrons and electrons) and two PF rings (electrons) has also worked well, giving a good reproducibility of each beam. These excellent situations are owing to not only the result of continuing efforts that the linac group has so far made to improving each hardware component, but also the fruits of introducing various feedback loops [53] (Fig. 27) in the orbit, energy and environmental parameters like the temperature and electricity along the linac. One example is stabilization of the primary electron beams for positron production, which was one of the key issues in the first stage of operation. We figured out that the stability of the beam intensity and orbit strongly depends on the timing of the grid pulser, which is, in turn, highly related to the temperature of the gun room. The room temperature is to be regulated more precisely in the near future, while a slow feedback loop was implemented so as to directly suppress the timing variation of the grid pulser, resulting in good beam stability for a high-intensity beam. We have thus more than 30 feedback loops in operation to assure stable injection into each ring.

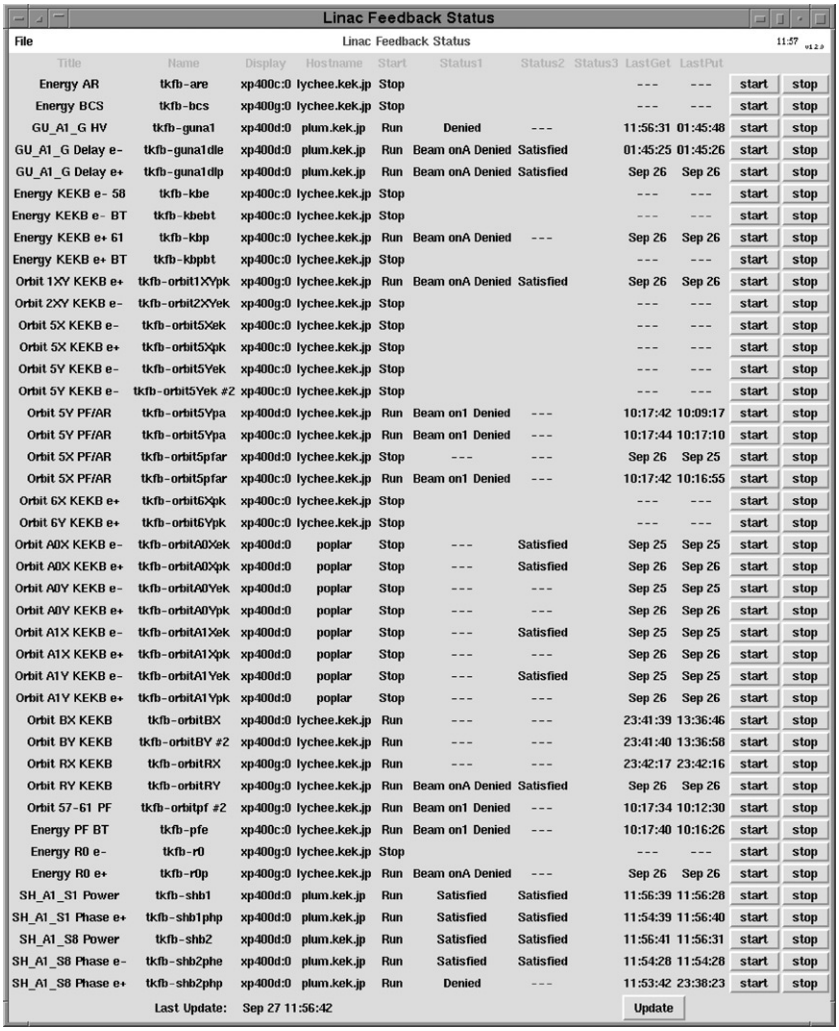

Fig. 27. Feedback loops.

11. Summary

The KEK electron/positron injector was successfully upgraded for the B-Factory project at KEK, while maintaining injection for synchrotron-orbit radiation experiments. To achieve 8-GeV electron beams, accelerator gain was increased from about 8 to 20 MeV/m as well as the accelerating modules from 40 to 55. The accelerating module has been stably operated for such a high gradient. The goal of the positron intensity upgrade was also achieved by accelerating an extremely intense electron beam of nearly 10 nC. To stabilize it, many beam-monitors and rf/timing monitors was newly constructed and a computer-controlled beam operation/feedback system were extensively developed. While switching beams into four kinds of rings, all beams are being injected smoothly. The injection time for the KEKB rings are adequate to integrate the luminosity for B-physics experiments.

Acknowledgements

The authors greatly appreciate Dr. G. Voss, who was the chairman of the KEKB accelerator review committee, and other members, especially Dr. J. Seeman and Dr. S. Wang, for helpful advice and encouragement for several years during the linac upgrade.

References

[1] J. Tanaka, et al., Nucl. Instr. and Meth. 177 (1980) 101.
[2] I. Sato, Nucl. Instr. and Meth. 177 (1980) 91.
[3] J. Tanaka, et al., Proceedings of the 1984 Linear Accelerator Conference, Darmstadt, Germany, 1984, pp. 475–479.
[4] A. Enomoto, et al., Nucl. Instr. and Meth. A 281 (1989) 1.
[5] A. Enomoto, Proceedings of the LINAC96, Geneva, Switzerland, 1996, pp. 633–637.
[6] A. Enomoto, et al., Proceedings of the EPAC2000, Vienna, Austria, 2000, pp. 993–995.
[7] Y. Ogawa, et al., Proceedings of the LINAC94, Tsukuba, Japan, 1994, pp. 535–537.
[8] S. Ohsawa, et al., Proceedings of the EPAC2000, Vienna, Austria, 2000, pp. 845–847.
[9] S. Yamaguchi, et al., Proceedings of the LINAC98, Chicago, IL, USA, 1998, pp. 558–560.
[10] J.Y. Choi, et al., Proceedings of the LINAC96, Geneva, Switzerland, 1996, pp. 340–342.
[11] T. Kamitani, et al., Proceedings of the LINAC94, Tsukuba, Japan, 1994, pp. 190–192.
[12] D.C. Carey, et al., SLAC-R-95-462, 1995.
[13] S. Yamaguchi, et al., Proceedings of the LINAC96, Geneva, Switzerland, 1996, pp. 346–348.
[14] T. Oogoe, et al., Proceedings of the LINAC94, Tsukuba, Japan, 1994, pp. 266–268.
[15] S. Yamaguchi, et al., Proceedings of the APAC98, Tsukuba, Japan, 1998, pp. 136–138.
[16] K. Kakihara, et al., Proceedings of the LINAC94, Tsukuba, Japan, 1994, pp. 567–569.
[17] Y. Ogawa, et al., Proceedings of the PAC95, Dallas, 1994, pp. 567–569.
[18] H. Hanaki, et al., Proceedings of the APAC98, Tsukuba, Japan, 1998, pp. 139–141.
[19] S. Fukuda, et al., Proceedings of the LINAC96, Geneva, Switzerland, 1996, pp. 187–189.
[20] H. Katagiri, et al., Proceedings of the APAC98, Tsukuba, Japan, 1998, pp. 142–144.
[21] S. Anami, et al., Proceedings of the 1981 Linear Accelerator Conference, Santa Fe, New Mexico, USA, 1981, pp. 177–179.
[22] S. Anami, et al., Proceedings of the Ninth Symposium on Accelerator Science and Technology, Tsukuba, Japan, 1993, pp. 125–127.
[23] T. Shidara, et al., Nucl. Instr. and Meth. A 279 (1989) 423.
[24] H. Honma, et al., Proceedings of the LINAC94, Tsukuba, Japan, 1994, pp. 436–438.
[25] T. Shintake, et al., Nucl. Instr. and Meth. A 363 (1995) 83.
[26] S. Fukuda, et al., Nucl. Instr. and Meth. A 368 (1996) 561.
[27] S. Fukuda, et al., Appl. Surf. Sci. 146 (1999) 84.
[28] S. Michizono, et al., Appl. Surf. Sci. 169–170 (2000) 742.
[29] H. Matsumoto, et al., Nucl. Instr. and Meth. A 330 (1993) 1.
[30] H. Hanaki, et al., Proceedings of the EPAC96, Barcelona, Spain, 1996, pp. 2003–2005.
[31] KEKB B-Factory Design Report, 1995, Chapter 12, p. 30.
[32] S. Ohsawa, et al., Proceedings of the LINAC94, Tsukuba, 1994, pp. 193–195.
[33] S. Ohsawa, et al., Proceedings of the PAC93, Washington, DC, USA, 1993, pp. 3087–3089.
[34] S. Ohsawa, et al., Proceedings of the LINAC90, Albuquerque, NM, USA, 1990, pp. 159–161.
[35] S. Ohsawa, et al., Proceedings of the PAC2001, Chicago, Illinois, USA, 2001, pp. 3284–3286.
[36] S. Ohsawa, et al., Proceedings of the HEACC92, Hamburg, Germany, 1992, pp. 135–137.
[37] Y. Ogawa, et al., Proceedings of the APAC98, Tsukuba, Japan, 1998, pp. 534–536.
[38] T. Suwada, et al., Nucl. Instr. and Meth. A 440 (2000) 307.
[39] N. Kamikubota, et al., Proceedings of the ICALEPCS99, Trieste, Italy, 1999, pp. 217–219.
[40] K. Furukawa, et al., Proceedings of the LINAC2000, Monterey, CA, 2000, pp. 633–635.
[41] T. Suwada, et al., Nucl. Instr. and Meth. A 396 (1997) 1.
[42] N. Iida, et al., Proceedings of the EPAC2000, Vienna, Austria, 2000, pp. 1738–1740.
[43] K. Furukawa, et al., Proceedings of the ICALEPCS91, Tsukuba, Japan, 1991, pp. 89–92.
[44] N. Kamikubota, et al., Nucl. Instr. and Meth. A 352 (1994) 131.
[45] K. Furukawa, et al., Proceedings of the ICALEPCS95, Chicago, USA, 1995, pp. 863–866.
[46] N. Kamikubota, et al., Proceedings of the ICALEPCS97, Beijing, China, 1997, pp. 351–353.
[47] K. Furukawa, et al., Proceedings of the ICALEPCS97, Beijing, China, 1997, pp. 146–149.
[48] K. Nakahara, et al., Nucl. Instr. and Meth. A 293 (1990) 446.
[49] I. Abe, et al., Proceedings of the ICALEPCS97, Beijing, China, 1997, pp. 519–521.
[50] URL:http://acc-physics.kek.jp/SAD/sad.html
[51] K. Furukawa, et al., Proceedings of the ICALEPCS99, Trieste, Italy, 1999, pp. 98–100.
[52] N. Kamikubota, et al., Proceedings of the APAC2001, Beijing, China, 2001, pp. 328–330.
[53] K. Furukawa, et al., Proceedings of the ICALEPCS99, Trieste, Italy, 1999, pp. 248–250.
[54] Y. Ogawa, et al., Proceedings of the Factories99, Tsukuba, Japan, 1999, pp. 64–69.
[55] T. Kamitani, et al., Proceedings of the APAC98, Tsukuba, Japan, 1998, pp. 429–430.